Anisotropic crystallization in solution processed chalcogenide thin film by linearly polarized laser

Tingyi Gu, Hyuncheol Jeong, Kengran Yang, Fan Wu, Nan Yao, Rodney D. Priestley, Claire E. White, and Craig B. Arnold

Citation: Appl. Phys. Lett. **110**, 041904 (2017); doi: 10.1063/1.4975067
View online: http://dx.doi.org/10.1063/1.4975067
View Table of Contents: http://aip.scitation.org/toc/apl/110/4
Published by the American Institute of Physics

Anisotropic crystallization in solution processed chalcogenide thin film by linearly polarized laser

Tingyi Gu,[1] Hyuncheol Jeong,[2] Kengran Yang,[3,4] Fan Wu,[5] Nan Yao,[5] Rodney D. Priestley,[2,5] Claire E. White,[3,4] and Craig B. Arnold[5,a)]
[1]*Electrical and Computer Engineering, University of Delaware, Newark, Delaware 19716, USA*
[2]*Chemical and Biological Engineering, Princeton University, Princeton, New Jersey 08544, USA*
[3]*Civil and Environmental Engineering, Princeton University, Princeton, New Jersey 08544, USA*
[4]*Andlinger Center for Energy and the Environment, Princeton University, Princeton, New Jersey 08544, USA*
[5]*Princeton Institute for the Science and Technology of Materials, Princeton University, Princeton, New Jersey 08544, USA*

(Received 12 December 2016; accepted 17 January 2017; published online 24 January 2017)

The low activation energy associated with amorphous chalcogenide structures offers broad tunability of material properties with laser-based or thermal processing. In this paper, we study near-bandgap laser induced anisotropic crystallization in solution processed arsenic sulfide. The modified electronic bandtail states associated with laser irradiation lead to a distinctive photoluminescence spectrum, compared to thermally annealed amorphous glass. Laser crystalized materials exhibit a periodic subwavelength ripple structure in transmission electron microscopy experiments and show polarization dependent photoluminescence. Analysis of the local atomic structure of these materials using laboratory-based X-ray pair distribution function analysis indicates that laser irradiation causes a slight rearrangement at the atomic length scale, with a small percentage of S-S homopolar bonds converting to As-S heteropolar bonds. These results highlight fundamental differences between laser and thermal processing in this important class of materials. *Published by AIP Publishing.* [http://dx.doi.org/10.1063/1.4975067]

Chalcogenide materials have the ability to transform among various states, ranging from random amorphous networks to atomically ordered crystalline states when exposed to modest energy such as that associated with optical or thermal processes.[1–5] These different structures typically exhibit significant optical refractive index contrast, as well as differences in electronic conductivities and other material properties. Among various tuning schemes, laser processing is especially interesting as it enables precise control of the amount of energy delivered into a specific targeted region. Such methods have been explored for tuning integrated photonic devices[6–13] as well as for controlling dichroism or polarization dependent photodarkening phenomena in these materials.[14–18] It has been shown that the precise atomic structure depends on the wavelength, duration, and intensity of laser irradiation.[18]

In the case of solution processed chalcogenide materials,[5,12] laser heating from above band-gap illumination has been shown to remove excess solvent related components to densify films and modify the surface chemistry and surface morphology.[3] It has been shown in arsenic sulfide (As_2S_3) that laser heating can induce thermal effects capable of breaking the chalcogenide-solvent bond. Furthermore, laser exposure can affect the structural properties of chalcogenide materials through polarization dependent athermal phenomena.[11] Such a process can cause redistribution of atomic clusters or chemical reactions leading to anisotropic properties.[14–18]

In this paper, we show that near-band gap laser irradiation can lead to structural changes unlike those associated with thermal processing. Beginning with a solution processed glass As_2S_3 film, laser processing results in crystallization and corresponding anisotropies in optical properties. Photoluminescence (PL) measurements show well-defined shifts in emission peaks relative to thermally annealed materials while pair distribution function (PDF) analysis highlights the changes in bonding structure within the films.

As_2S_3 solution is prepared as in prior work by dissolving amorphous As_2S_3 powder in propylamine.[12] This solution is then spin-cast or drop coated on a substrate (TEM grid or silica microscope slide) and thermally processed at different temperatures as specified in the results. Fig. 1(a) shows the

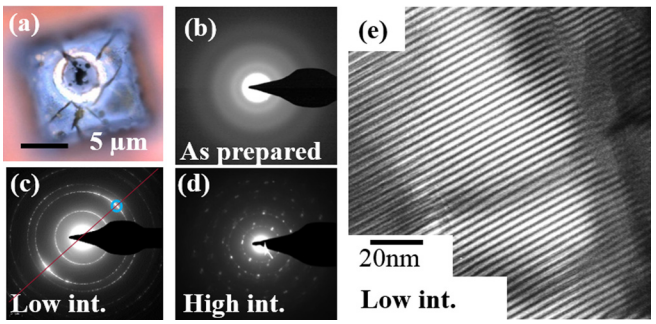

FIG. 1. Laser Gaussian beam induced pattern on the chalcogenide thin film. (a) Optical image of the solution processed As_2S_3 film drop-cast on the TEM grid, observed under a 100× microscope after a laser exposure of 10 s, with an average power of 160 $\mu W/\mu m^2$. Scale bar: 5 μm. (b) Electron diffraction pattern for the region before laser crystallization and (c) crystallized region near the center of the beam (40 $\mu W/\mu m^2$). The red line shows the preferred nanocrystal orientation. (d) The crystallized region after laser exposure with 160 $\mu W/\mu m^2$. (e) A corresponding dark-field image showing the real-space structure as in (c), through the aperture in the blue circle.

a)Author to whom correspondence should be addressed. Electronic mail: cbarnold@princeton.edu

optical image of As_2S_3 drop cast on a TEM grid (carbon coated, copper grid). The TEM grid size is 10 μm × 10 μm. A 532 nm laser beam and Gaussian beam profile are concentrated in the middle of the film, and the bright circles in Fig. 1(a) indicate the extent of the laser beam. The dark spot in the center of the laser exposed region shows the laser crystalized area. TEM (Phillips CM200) is performed at 200 keV in bright-field, dark-field, and diffraction conditions. The diffraction pattern of the unexposed material shows blurry rings indicating the amorphous nature of the solution processed As_2S_3 (Fig. 1(b)). In comparison, the diffraction pattern from the center of the laser-exposed area shows a clear crystalline structure formed under both low (40 $\mu W/\mu m^2$) (Fig. 1(c)) and high (160 $\mu W/\mu m^2$) (Figure 1(d)) laser intensities. The measured lattice spacings for the low intensity exposure (2.636 Å and 1.512 Å) correspond to polycrystalline As_4S_4 (2.636 Å and 1.513 Å). Also, the polycrystalline structure shows a preferred orientation indicated with an intensity enhancement in the diffraction as shown in Fig. 1(c) (marked with a circle). The TEM diffraction pattern of high laser intensity exposure shows distinct periodic spots indicating a single crystal type structure (Fig. 1(d)). As a small aperture is placed covering only the diffracted beams in the circled region in Fig. 1(c), a dark-field image (Fig. 1(e)) is formed, which shows a Moire pattern of ~10 nm spacing due to the overlap of As_4S_4 nanostructure crystal layers with preferred orientations.

A Bruker D8 Advance X-ray diffractometer was used to obtain PDFs of the As_2S_3 system in order to probe its atom-atom correlations. The As_2S_3 solution is dried in a ceramic pestle and the resulting powder is loaded into a 2.5-in. long polyimide capillary and sealed using quick-setting transparent epoxy. The material is then uniformly exposed to a 30 $\mu W/\mu m^2$ (low intensity) 532 nm laser for approximately 5 min and 120 $\mu W/\mu m^2$ (high intensity) for the same duration. Ag Kα radiation is used, which has a smaller wavelength compared to Cu radiation, and hence provides a broader Q range. A step size of 0.050°, along with a count time per step of 30 s, and a 2θ range of 3° to 130° are used. The PDF, $G(r)$, was obtained by taking a sine Fourier transform of the measured total scattering function, $S(Q)$, as shown in Equation (1).[19]

$$G(r) = \frac{2}{\pi}\int_{Q_{min}}^{Q_{max}} Q[S(Q) - 1]\sin(Qr)dQ, \qquad (1)$$

where Q is the momentum transfer given by $Q = 4\pi\sin\theta/\lambda$. Standard data reduction procedures are followed to obtain the PDF using PDFgetX2,[20] with a Q_{max} of ~14.4 Å^{-1}. Prior to calculation of the PDF, the total scattering function is multiplied by a Lorch window function[21] to improve the signal/noise at the expense of real-space resolution.

Fig. 2 displays the X-ray PDF data for the solution processed sample () together with the laser exposed samples at two different intensities. In contrast to the TEM results, where it was clear that laser exposure led to local alterations of the atomic structure (Fig. 1), the PDF data show minimal changes to the amorphous atomic structure as a result of laser exposure. The first atom-atom correlation in the X-ray PDF at 2.26 Å is assigned to the As-S bond length (denoted as (i) in Fig. 2), while the second correlation at 3.45 Å is attributed to the atom-atom distances of As-As, S-S, and 2nd nearest-neighbor As-S (denoted as (ii) in Fig. 2).[22] Slight changes to the ratio of the peak intensities at these locations, $G(i)/G(ii)$, as a result of laser exposure, are indicative of rearrangements to the atomic structure. As the intensity of laser exposure increases, the $G(i)/G(ii)$ ratio increases, implying that some of the S-S homopolar bonds are being converted to As-S heteropolar bonds. This observation agrees with the electron diffraction patterns shown in Fig. 1, where upon laser exposure the structure becomes more ordered with a layered anisotropic structure. Hence, the PDF results indicate that exposure to radiation causes the structure to rearrange although no sign of crystallization is visible in the data using this bulk analysis technique.

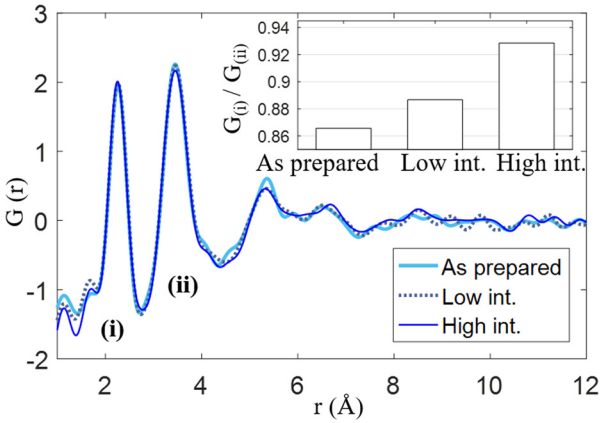

FIG. 2. Laboratory X-ray PDF data for solution processed sample before laser exposure (as prepared), after low intensity laser exposure (532 nm, 30 $\mu W/\mu m^2$) and high intensity laser exposure (532 nm, 120 $\mu W/\mu m^2$). Inset: The peak intensity ratio of the first nearest neighbor correlation intensity (i) to the second (ii).

Fig. 3(a) shows Fourier transform infrared spectra (FTIR) of as-spin coated arsenic sulfide without thermal or laser processing and the same material followed by thermal annealing at 110 °C, 160 °C, and 185 °C, respectively. The broad absorption at 2200–3100 cm^{-1}, indicative of amine molecules, gradually weakens as the material is annealed at higher temperature. The two absorption peaks in the range of 1300–1700 cm^{-1}, representing solvent species in the sample, disappear entirely at the annealing temperature of 185 °C. The Differential Scanning Calorimetry (DSC) thermograms of solution-processed As_2S_3 powders (red curve in Fig. 3(d)) exhibit a broad endothermic peak around 135 °C, while the same sample with pre-annealing at 120 °C for 5 h does not (blue line in Fig. 3(d)). We expect that the endothermic peak corresponds to the decomposition of sulfur bonds associated with the propylamine dissolution and the removal of H in the form of H_2S as proposed by Chern *et al.*[23] In addition, we find that temperature around 180–190 °C induced another structural change of the material, as supported by noisy peaks in the DSC trace of solution-processed As_2S_3 (Fig. 3(d)). In comparison to the DSC trace of raw As_2S_3 (black curve in Figure 3(d)), this temperature matches the expected glass transition (T_g) (Fig. 3(e)) at which the material becomes liquid like from the glassy state. T_g in the raw material is measured to be near 191.7 °C. The structural changes captured

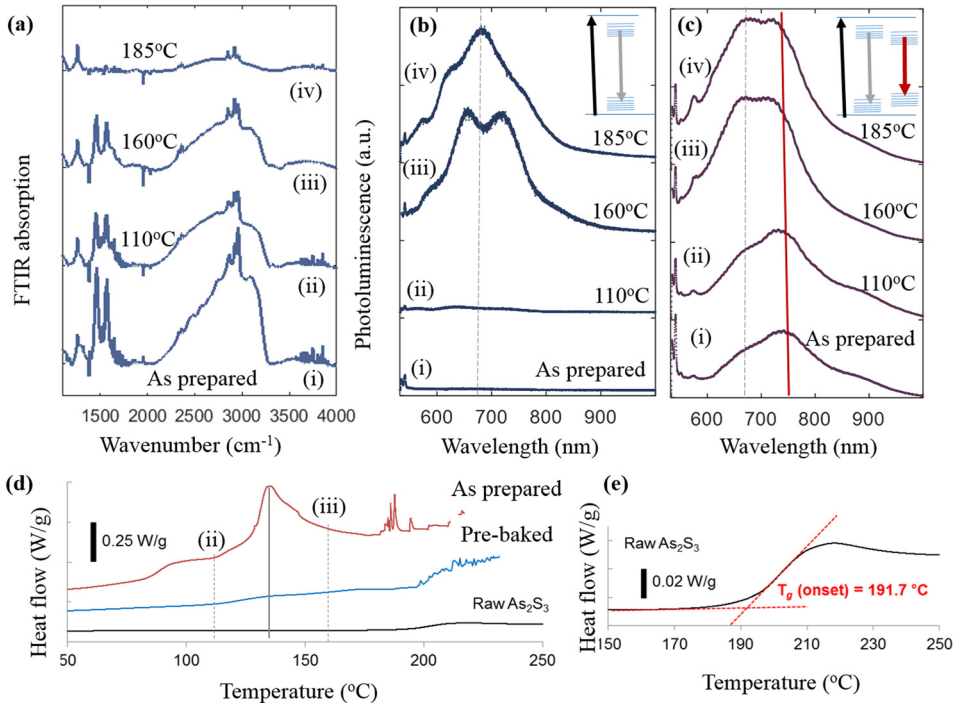

FIG. 3. Photoluminescence of laser and thermal induced defects. (a) FTIR measurement of the spin coated sample before (i) and after annealing in a nitrogen environment at (ii) 110 °C, (iii) 160 °C, and (iv)185 °C for 5 h. Note that all curves have the same scale but are shifted on the y-axis for clarity. (b) Photoluminescence of the corresponding samples shown in (a), normalized to the intensity of Raman emission peak near 550 nm. The grey dashed line marks the center wavelength of the thermal induced defect state. Inset: band diagram and absorption (black arrow) and emission (grey arrow) from the thermal induced defects. Spectra are individually normalized and shifted for clarity. (c) Photoluminescence of the spin coated sample after 40 μW/μm^2 laser exposure for 10 s. The grey dashed line and red solid line mark the center wavelength of the amorphous thermally annealed sample and laser crystallized structure, respectively. Inset: absorption (black arrow) and emission from thermal induced (grey arrow) and laser induced (red) defects. (d) Differential scanning calorimetry (DSC) thermograms of raw (black), solution processed (blue), and pre-annealed (120 °C for 5 h in a vacuum of solution processed sample) arsenic sulfide. The heating rate is 10 °C/min. The solid gray line marks the transition temperature at which the solvent bond breaks off. The grey dashed lines show the temperature below (ii) and above (iii) the transition temperature, as marked in (a)–(c). (e) Magnified DSC measurement showing the glass transition of raw arsenic sulfide.

by DSC are consistent with the FTIR measurement results, where the FTIR peaks representing the solvent bonds disappear after annealing beyond 135 °C of the endothermic peak.

The PL spectra were collected by coupling the light scattered from the sample to a Horiba Raman spectrometer through a 100× objective, focusing the probe laser (532 nm) spot to ~1.5 μm^2. The excitation laser intensity is controlled below 0.4 μW/μm^2 to minimize nonlinear response and minimize any subsequent modifications to the material. The presence of the solvent in As_2S_3 prevents photoluminescence, and only samples annealed above DSC measured endothermic peak around 135 °C exhibit a strong photoluminescence signal. As the glass restructures with thermal annealing at 160 °C and 185 °C, the defect levels in solution processed As_2S_3 give rise to a broadband emission spectrum in the visible band, centered at 680 nm. In the band diagram inset of Figs. 3(b) and 3(c), the black arrow conceptualizes the As_2S_3 absorption with near bandgap energy, and the grey arrows show photoluminescence from the defects levels. Laser crystallized As_4S_4 has particular energy levels for radiative recombination compared to thermally processed samples and the PL spectrum shows significant differences (Fig. 3(c) vs 3(b)). In particular, the laser irradiated samples show a red shift in the center of the PL spectrum from 680 nm for the thermally processed samples to 750 for the laser processed samples.

Thermal annealing removes solvent species to form isotropic amorphous films, while the polarized laser crystallizes the chalcogenide material (Fig. 1(e)). The anisotropy of the crystal would be expected to exhibit an excitation polarization dependence in the PL spectrum. After crystallization of the material by high intensity laser (532 nm), we probe the modified PL of the crystallized region on the same set-up configuration but reduce the laser power to monitor the PL spectrum. Figure 4(a) shows the PL spectrum from laser crystallized materials under different excitation polarizations of 0°, 45°, 90°, 135°, and 180°. The polarization degree is relative to the one of crystallization laser. We see that the maximum emission intensity occurs for 90° showing a 50%

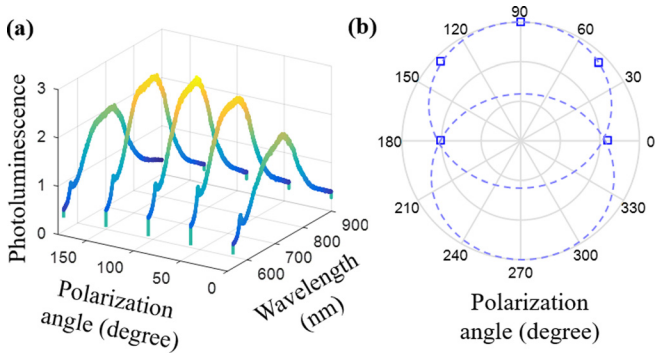

FIG. 4. Photoluminescence spectra of the laser crystallized chalcogenide. (a) Photoluminescence spectra and (b) intensity versus relative polarization angle to the crystallization laser. The blue squares are experimental data and the dashed circles are fitted circles.

enhancement of photoluminescence relative to the parallel polarization (0°) further confirming the preferred anisotropy in the polycrystalline structure shown in Fig. 1(c).

We studied the localized atomic structure change in solution processed arsenic sulfide by near bandgap laser exposure. Fundamental differences between thermal and laser-based processing are observed by thermal, optical, X-ray, and electron microscopy characterization corresponding to differences in the structural properties of the material. These locally crystallized anisotropic chalcogenide materials could be incorporated for designing new components in integrated photonic devices.

The authors thank Professor Yueh-Lin Loo of Princeton University and facility at Imaging and Analysis Center at Princeton University for their intriguing discussions. This work was supported by NSF through the MIRTHE Center (Grant No. EEC-0540832) and MRSEC Center (Grant No. DMR-1420541). T.G. acknowledges partial support from the School of Engineering and Department of Electrical and Computer Engineering at University of Delaware.

The authors declare no competing financial interest.

[1]V. Weidenhof, I. Friedrich, S. Ziegler, and M. Wuttig, "Laser induced crystallization of amorphous $Ge_2Sb_2Te_5$ films," J. Appl. Phys. **89**, 3168–3176 (2001).
[2]H. F. Hamann, M. O'Boyle, Y. C. Martin, M. Rooks, and H. K. Wickramasinghe, "Ultra-high-density phase-change storage and memory," Nat. Mater. **5**, 383–387 (2006).
[3]D. Savytskii, B. Knorr, V. Dierolf, and H. Jain, "Challenges of CW laser-induced crystallization in a chalcogenide glass," Opt. Mater. Express **3**, 1026–1038 (2013).
[4]C. Markos, "Thermo-tunable hybrid photonic crystal fiber based on solution-processed chalcogenide glass nanolayers," Sci. Rep. **6**, 31711 (2016).
[5]S. Song, J. Dua, and C. B. Arnold, "Influence of annealing conditions on the optical and structural properties of spin-coated As_2S_3 chalcogenide glass thin films," Opt. Express **18**, 5472–5480 (2010).
[6]C. Markos, "Photo-induced changes in a hybrid amorphous chalcogenide/silica photonic crystal fiber," Appl. Phys. Lett. **104**, 011114 (2014).
[7]D. Sridharan, E. Waks, G. Solomon, and J. T. Fourkas, "Reversible tuning of photonic crystal cavities using photochromic thin films," Appl. Phys. Lett. **96**, 153303 (2010).
[8]A. Faraon, D. Englund, D. Bulla, B. Luther-Davies, B. J. Eggleton, N. Stoltz, P. Petroff, and J. Vučković, "Local tuning of photonic crystal cavities using chalcogenide glasses," Appl. Phys. Lett. **92**, 043123 (2008).
[9]A. Canciamilla, F. Morichetti, S. Grillanda, P. Velha, M. Sorel, V. Singh, A. Agarwal, L. C. Kimerling, and A. Melloni, "Photo-induced trimming of chalcogenide-assisted silicon waveguides," Opt. Express **20**, 15807–15817 (2012).
[10]A. Canciamilla, S. Grillanda, F. Morichetti, C. Ferrari, J. Hu, J. D. Musgraves, K. Richardson, A. Agarwal, L. C. Kimerling, and A. Melloni, "Photo-induced trimming of coupled ring-resonator filters and delay lines in As_2S_3 chalcogenide glass," Opt. Lett. **36**, 4002–4004 (2011).
[11]C. Lu, D. Recht, and C. B. Arnold, "Generalized model for photoinduced surface structure in amorphous thin films," Phys. Rev. Lett. **111**, 105503 (2013).
[12]Y. Zha, M. Waldmann, and C. B. Arnold, "A review on solution processing of chalcogenide glasses for optical components," Opt. Mater. Express **3**, 1259–1272 (2013).
[13]C. D'Amico, C. Caillaud, P. K. Velpula, M. K. Bhuyan, M. Somayaji, J.-P. Columbier, J. Troles, L. Calvez, V. Nazabal, A. Boukenter, and R. Stoian, "Ultrafast laser-induced refractive index changes in $Ge_{15}As_{15}S_{70}$ chalcogenide glass," Opt. Mater. Express **6**, 1914–1928 (2016).
[14]G. Chen, H. Jain, M. Vlcek, S. Khalid, J. Li, D. A. Drabold, and S. R. Elliott, "Observation of light polarization-dependent structural changes in chalcogenide glasses," Appl. Phys. Lett. **82**, 706–708 (2003).
[15]V. Lyubin, M. Klebanov, M. Mitkova, and T. Petkova, "Polarization-dependent, laser-induced anisotropic photocrystallization of some amorphous chalcogenide films," Appl. Phys. Lett. **71**, 2118–2120 (1997).
[16]V. M. Lyubin and M. L. Klebanov, "Laser-induced anisotropic absorption, reflection, and scattering of light in chalcogenide glassy semiconductors," Semiconductors **32**, 817–823 (1998).
[17]K. Richardson, T. Cardinal, M. Richardson, A. Schulte, and S. Seal, "Engineering glassy chalcogenide materials for integrated optics applications," in *Photoinduced metastability in Amorphous Semiconductors*, edited by A. V. Koloboc (Wiley-VCH, Weinheim, 2003).
[18]K. Antoine, H. Jain, M. Vlcek, S. D. Senanayake, and D. A. Drabold, "Chemical origin of polarization-dependent photoinduced changes in an $As_{36}Se_{64}$ glass film via in situ synchrotron x-ray photoelectron spectroscopy," Phys. Rev. B **79**, 054204 (2009).
[19]E. Takeshi and S. J. L. Billinge, *Underneath the Bragg Peaks: Structural Analysis of Complex Materials* (Elsevier, 2003).
[20]X. Qiu, J. W. Thompson, and S. J. L. Billinge, "PDFgetX2: A GUI-driven program to obtain the pair distribution function from X-ray powder diffraction data," J. Appl. Crystallogr. **37**, 678 (2004).
[21]E. Lorch, "Neutron diffraction by germania, silica and radiation-damaged silica glasses," J. Phys. C: Solid State Phys. **2**, 229–237 (1969).
[22]D. J. E. Mullen and W. Nowacki, "Refinement of crystal structures of realgar, AsS and orpiment, As_2S_3," Z. Kristallogr. **136**, 48–65 (1972).
[23]G. C. Chern, I. Lauks, and A. R. McGhie, "Spin coated amorphous chalcogenide films: Thermal properties," J. Appl. Phys. **54**, 4596–4601 (1983).